Research in Astronomy and Astrophysics, 22:122001 (14pp), 2022 December https://doi.org/10.1088/1674-4527/ac97d1

From Solar System to Exoplanets: What can we learn from Planetary Spectroscopy?

Therese Encrenaz
LESIA, Paris Observatory-PSL Université, CNRS, Sorbonne Université, Université de Paris, Paris, France; therese.encrenaz@obspm.fr
Received 2022 July 27; revised 2022 September 26; accepted 2022 October 4; published 2022 November 16

Abstract

The purpose of this paper is to address the question: Using our knowledge of infrared planetary spectroscopy, what can we learn about the atmospheres of exoplanets? In a first part, a simplified classification of exoplanets, assuming thermochemical equilibrium, is presented, based on their masses and their equilibrium temperatures, in order to propose some possible estimations about their atmospheric composition. In the second part, infrared spectra of planets are discussed, in order to see what lessons can be drawn for exoplanetary spectroscopy. In the last part, we consider the solar system as it would appear from a star located in the ecliptic plane. It first appears that the solar system (except in a few specific cases) would not be seen as a multiple system, because, contrary to many exoplanetary systems, the planets are too far from the Sun and the inclinations of their orbits with respect to the ecliptic plane are too high. Primary transit synthetic spectra of solar system planets are used to discuss the relative merits of transmission and direct emission spectroscopy for probing exoplanetary atmospheres.

Key words: planets and satellites: atmospheres – planets and satellites: composition – (stars:) planetary systems

1. Introduction

Over the past twenty-five years, over five-thousand extrasolar planets have been discovered. Following the first detection of 51 Peg b (Mayor & Queloz 1995), the radial velocity method first led to the detection of hundreds of giant exoplanets in the close vicinity of their host star—what we now call the "hot Jupiters," a new category of planets which do not exist in our solar system. Starting from 1999 (Charbonneau et al. 2000), the method of transits, using both ground-based and space means, allowed the discovery of also smaller objects—Neptunes and super-Earths—all close to their host stars. The combination of these two methods gives access to the periods of the objects, their masses and radii. In the meantime, the gravitational microlensing technique gave an insight on a new population of more distant exoplanets, often located at several thousand parsecs (Beaulieu et al. 2006). Since 2005 (Chauvin et al. 2005), the imaging technique, used on very large ground-based telescopes, allows the direct detection of young and warm giant exoplanets at some distance (typically tens or hundreds of au) from their host star. All these observable means have given us a broad picture of the exoplanets which demonstrates the wide variety of their orbital and physical conditions. We have seen that multiple systems (with more than one planet) are frequent (over 800), but we have found no equivalent of our solar system so far. In addition, thanks to transit spectroscopic observations, we now have some information about the chemical composition of about a hundred exoplanet atmospheres.

The aim of this paper is to address the following question: Using our knowledge of solar system planets, what can we learn about the atmospheres of exoplanets? This question will be discussed along three directions. In a first part, we will start from our understanding of the solar system formation scenario to make a guess on what could be the atmospheric composition of an exoplanet, on the basis of its mass and the distance to its host star. In a second part, we will discuss what we can expect for the infrared spectra of exoplanets, on the basis of our knowledge of infrared planetary spectroscopy. Finally, in the third part, we will consider the solar system as if it were seen from a distant star located in the ecliptic plane, in order to estimate the information which could be retrieved from transit observations. Conclusions and perspectives will be discussed in the last part.

2. Atmospheric Composition of Exoplanets

In this section, we consider a transiting exoplanet, for which the mass and the distance to its host-star are known, and we wonder if we can guess what could be its atmospheric composition. To do so, we start from the formation scenario of the solar system. It is generally accepted that the Sun (like most stars) was formed following the collapse of a rotating nebula into a protosolar disk. According to the so-called core-accretion model (Mizuno 1980; Pollack et al. 1996), the solar system planets were formed in this disk from the progressive accretion of solid material, the planetesimals. The nature of the planet then depends upon the nature of the solid material available in

its environment. Two cases can be considered: (1) within about 3 au from the Sun, where the temperature is higher than 200 K, the only solid matter is made of the refractory materials (silicates, oxydes, metals, ...); these materials are made of heavy atoms which, according to the cosmic abundances of the elements, are not abundant in the universe, because their formation through stellar nucleosynthesis requires a large amount of energy. The amount of solid matter available to build planetary cores is thus limited, but these cores are dense. As a result, the rocky planets, or terrestrial planets, formed by this process, are small and dense. (2) At further distance to the Sun, beyond about 3 au (T lower than 200 K), the temperature is low enough for small molecules (H_2O, CH_4, NH_3, …) to be in the form of ices. These ices, made of relatively light elements (C, N, O, ...), are much more abundant than the heavy atoms, and can build large cores whose mass can reach ten terrestrial masses. According to theoretical models, this mass is sufficient for the gravity field of the core to capture the surrounding material, mostly composed of hydrogen and helium. This explains the formation of giant planets, with a large size and a low density. In addition, the collapse of the surrounding sub-nebula along the equatorial plane of the giant planet makes possible the formation, in this plane, of regular satellites and rings. The limit between these two kinds of planets is marked by the condensation of small molecules (the "ice line"). Actually, water has a major role in this process, because H_2O is relatively abundant and, by far, the first molecule to condense as the temperature decreases (i.e., as the distance to the Sun increases), so the ice line actually corresponds to water condensation.

Now let us consider what could be the chemical atmospheric composition of each class of planet. Assuming thermochemical equilibrium, in the presence of water, we can expect, at high pressures and low temperatures, carbon to be in the form of methane CH_4 and nitrogen to be in the form of ammonia NH_3, while, under opposite conditions, CO and N_2 respectively are expected (Lewis 1995, Figure 1), according to the following equilibrium reactions

$$CH_4 + H_2O \longrightarrow CO + 3H_2$$
$$2NH_3 \longrightarrow N_2 + 3H_2$$

which evolve toward the left-hand side for high pressures and low temperatures, and toward the right-hand side under opposite conditions. The first case applies to the giant planets which are cold and massive, and have a hydrogen-rich atmosphere with methane, ammonia and water. In the case of the terrestrial planets, another reaction transforms CO into CO_2

$$CO + H_2O \longrightarrow CO_2 + H_2$$

so we can expect, to first order, a (CO_2, N_2, H_2O) atmosphere. Hydrogen escapes, because the gravity field of these planets is not sufficient to retain it. This composition is expected to have been one of the primitive atmospheres of terrestrial planets; these atmospheres later evolved due to specific physicochemical processes (loss of water on Mars and Venus, apparition of oxygen on the Earth).

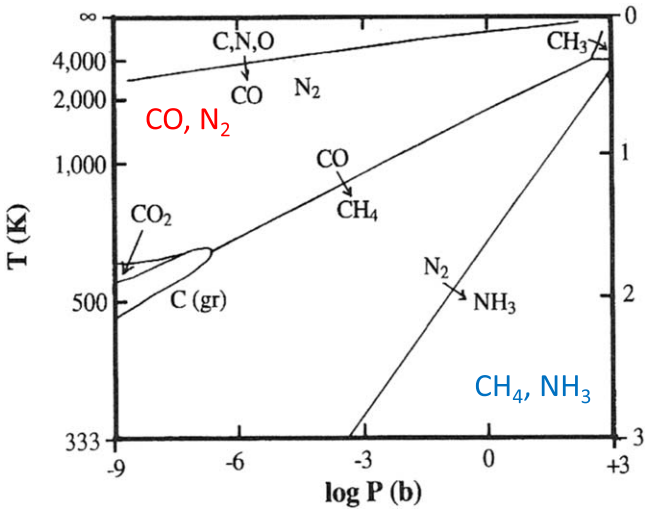

Figure 1. Carbon and nitrogen chemistry as a function of pressure (log scale in bars, abscissa) and temperature (in K, ordinate). The figure is adapted from J. S. Lewis, "Physics and Chemistry of the solar system," Academic Press, 1995.

Let us consider now the inventory of the solar system bodies. We can make a simple classification on the basis of their equilibrium temperature and their mass, considering two thresholds: for the temperature, the one of the ice line T_{il} (about 200 K) and, for the mass, the value of 10 terrestrial masses (M_c), which (to first order) separates the rocky/icy bodies from the giant planets. Considering the bodies surrounded with an atmosphere, we find three categories: (1) the rocky planets (T larger than T_{il}, M lower than M_c) with an atmosphere dominated by CO_2, N_2, H_2O; (2) the icy bodies (Titan, Triton: T lower than T_{il}, M lower than M_c) with a (CH_4, N_2) atmosphere (N_2 in this case might come from the photolysis of NH_3); (3) the giant planets (T lower than T_{il}, M larger than M_c with a (H_2, CH_4, NH_3, H_2O) atmosphere (with water being mostly in condensed form).

Now we come back to our exoplanet. Knowing the distance to its host-star (D) and the spectral type of this star, we can estimate its equilibrium temperature (T) on the basis of the following equation (Tinetti et al. 2013; Encrenaz & Lequeux 2022)

$$[F/D^2](1 - a) = 4\sigma T^4$$

where F is the stellar flux, a is the albedo and σ is the Planck constant. The value of a is unknown; value of 0.3, typical of solar system planets, can be used (anyway, its dependence on T is minor). The factor 4 corresponds to a fast-rotating planet which radiates over 4π sr the flux received on the dayside hemisphere.

Knowing the mass and the temperature of the exoplanet, we can locate it on the (T, M) diagram and make a guess about its

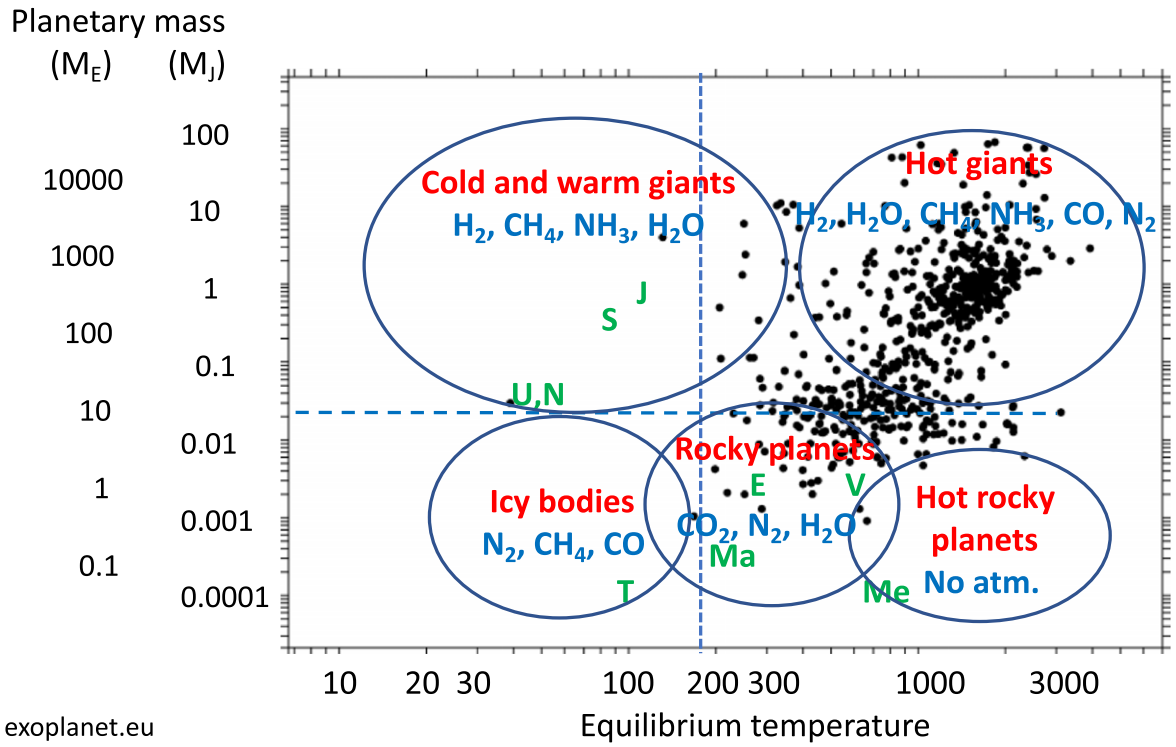

Figure 2. The distribution of exoplanets as a function of their equilibrium temperature (log scale in K, abscissa) and their mass (log scale, in terrestrial masses and in Jovian masses, ordinate). Various classes are indicated in red, with their tentative atmospheric composition in blue. The solar system planets are indicated in green.

atmospheric composition (Figure 2). Regarding the exoplanet distribution in this diagram, we have little information about the cold objects, which is obviously an observational bias as they are distant from their host-stars and their intrinsic signal is weak. We note that the new population of young giant exoplanets, warm but far from their star, recently discovered by imaging techniques, is not considered in this discussion. In our diagram, the warm and hot objects are well populated, but it immediately appears that their distribution does not match our categories: there is no clear separation between the rocky exoplanets and the giants ones, as observed in the solar system (a gap might exist, however, between 1.5 and 2 Earth masses, as suggested by Fulton et al. 2017 using the California-Kepler survey).

What are the possible reasons for this difference? A first reason could be a planetary formation scenario different from the core accretion model which applies to solar system planets, based on gravitational instabilities (Cameron 1988) but, more likely, the main reason is the migration process, not considered in our simple model, which is known to be a major evolutionary process in exoplanetary systems: it is now generally accepted that, in many cases, a giant exoplanet is formed within a protoplanetary disk beyond the ice line, creates a gap within the protoplanetary disk and migrates toward the star due to its interaction with the disk (Trilling et al. 2002). It is interesting to note that the migration process, identified at the time of the discovery of the first hot Jupiters, has been also identified, although in a less extreme form, in the case of the solar system. According to the "Nice model" (Tsiganis et al. 2005; Walsh et al. 2011), Jupiter first formed at about 3 au just beyond the ice line, moved toward the Sun down to the orbit of Mars but the arrival of Saturn made the two giant planets move back toward the external solar system. This scenario is not proven, as it is the result of numerical simulations, but it has the advantage of accounting for a number of observations, in particular the spatial distribution of some families of small bodies. This topic is an on-going field of research (Morbidelli et al. 2022), as this solution is not unique, and other alternative scenarios have been proposed to account for the present distribution of small bodies in the solar system.

In addition to the migration issue, there is another assumption that may not be always valid, which is thermochemical equilibrium. We have examples of hot Jupiters displaying an atmospheric composition which is different from the predictions of thermochemical equilibrium. Indeed, in the case of hot Jupiters in the vicinity of solar-type stars, carbon is expected to be in the form of CO within 0.05 au, and CH_4 beyond 0.10 au (Perryman 2011). In the case of HD 209458 b and HD 189733 b, our two brightest and most observed targets, both CH_4 and CO are observed. It is interesting to note that, in the case of the

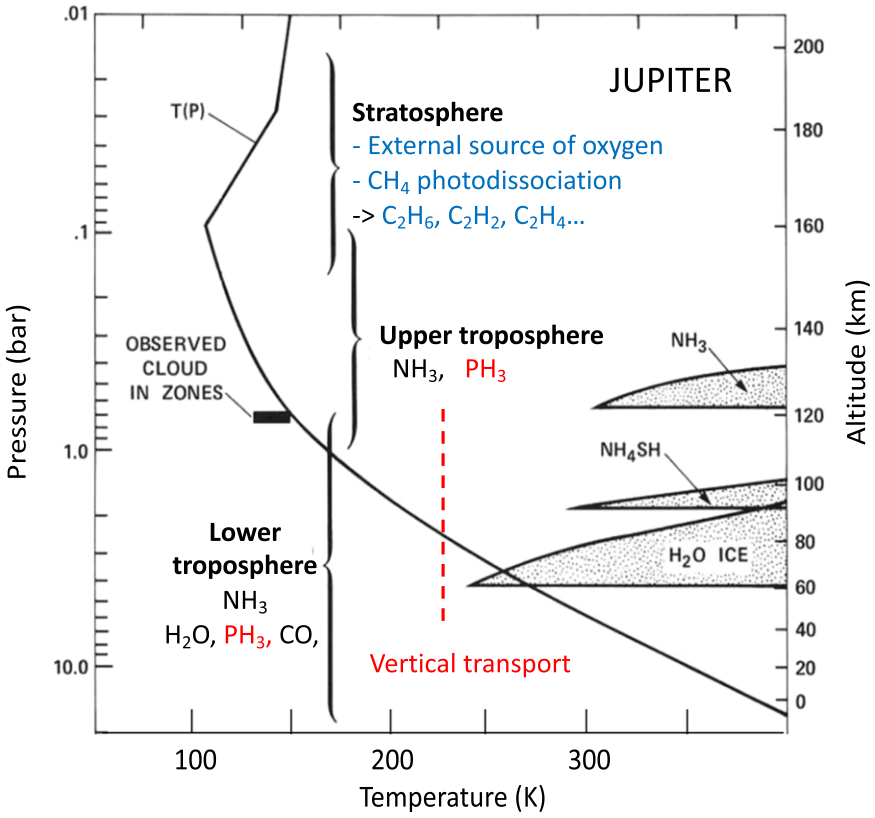

Figure 3. Departures from thermochemical equilibrium in the atmosphere of Jupiter. In the stratosphere, the causes are (1) the external influx of oxygen-bearing molecules (H_2O and CO, leading to the formation of CO_2, also possibly coming from the outside), and (2) the photodissociation of methane CH_4, leading to the formation of several hydrocarbons (C_2H_6, C_2H_2, C_2H_4, ...). In the troposphere, vertical transport is responsible for the presence of phosphine PH_3 at observable levels. Such processes could possibly occur in giant hydrogen-rich exoplanets.

solar system planets, departures from thermodynamical equilibrium are also observed (Figure 3). In the stratospheres of the giant planets, in particular, oxidized molecules have been found (H_2O, CO, CO_2), as a result of an incoming flux of oxidized material, coming from comets, micrometeorites or nearby rings and satellites (Feuchtgruber et al. 1997); in addition, the photolysis of methane leads to the formation of various hydrocarbons, including C_2H_2, C_2H_4 and C_2H_6. In the upper troposphere of Jupiter and Saturn, another disequilibrium species is observed, phosphine PH_3. This molecule is expected to be present in the deep atmosphere but, at a temperature below 800 K, is expected to react with H_2O to form P_4O_6. Its presence near the tropopause is interpreted as the signature of a strong vertical transport which carries the phosphine up to the tropopause in a timescale shorter than the destruction time of the molecule (Lewis 1995). Such mechanisms might also be at work in the case of giant exoplanets.

3. Infrared Spectra of (Exo)Planets

As for any solar system object, the infrared spectrum of a planet is made of two components: the reflected solar flux, and the thermal emission, corresponding to the part of the solar flux which is absorbed by the planet and converted into thermal heat. To first approximation, the solar component is a blackbody at the solar temperature (5770 K) and peaks at 0.5 μm; the planetary signatures (spectral lines from the atmosphere or mineralogic bands from the surface) appear in absorption in front of the solar continuum. The thermal emission is, to first order, a blackbody corresponding to the equilibrium temperature of the planet, as defined above. In the solar system, the equilibrium temperature is typically between 50 and a few hundred K, so that its maximum lies in the mid-infrared range (Figure 4). For a planet with an atmosphere, in the thermal regime, the outgoing flux is calculated from the radiative transfer equation (see e.g., Lissauer & de Pater 2013; Encrenaz & Lequeux 2022). An important parameter is the optical depth τ which is the integral of the extinction coefficient along the line of sight. For a given atmospheric constituent, at a given atmospheric layer, the extinction coefficient is the product of the molecular absorption coefficient (known from spectroscopic databases) and the density of the molecule. It can be shown that the outgoing flux corresponds to the blackbody radiation at the

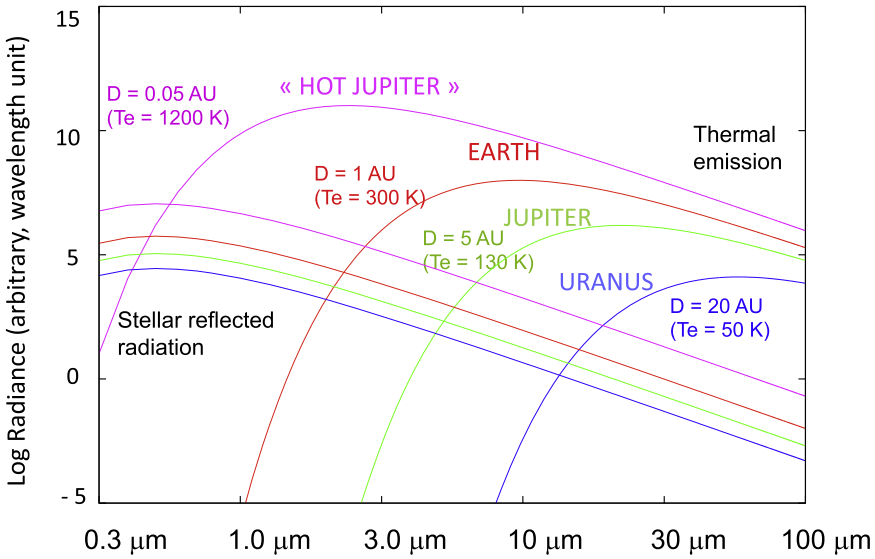

Figure 4. The two components of the infrared spectrum of an (exo)planet around a solar-type star. The reflected stellar component, represented by a blackbody at 5770 K multiplied by an albedo of 0.3 (a typical value for solar system objects), peaks at a wavelength of 0.5 μm. The thermal component is represented as a blackbody at the equilibrium temperature of the exoplanet (see Section 1). This is an approximation, as this blackbody is actually modulated by atmospheric lines, appearing in emission and/or in absorption, depending on the thermal gradient of the emitting region (stratosphere or troposphere, see text).

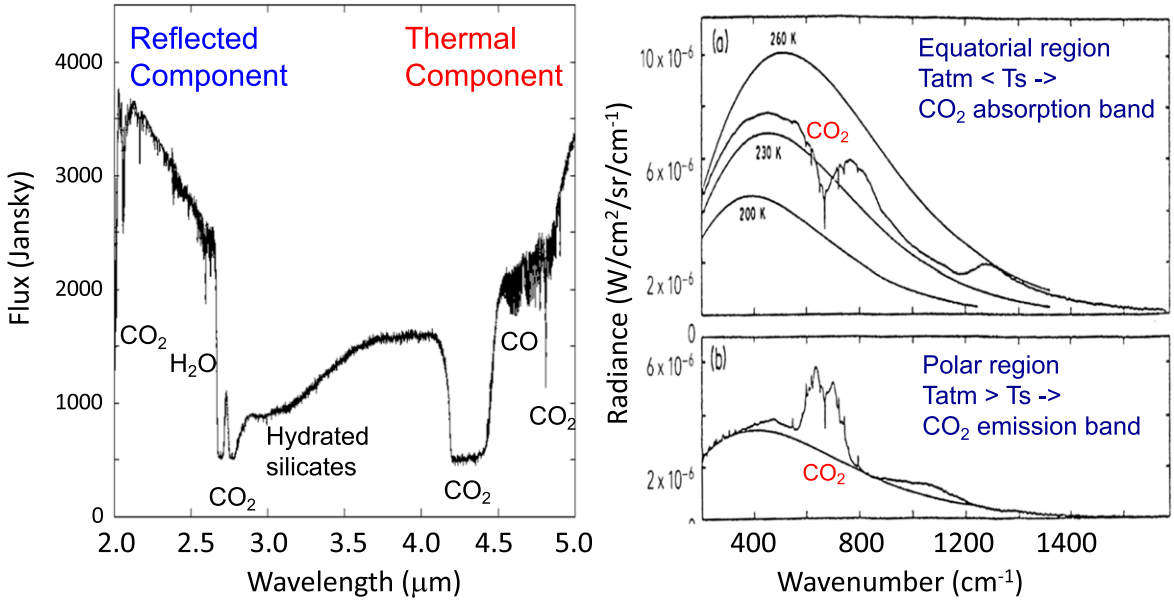

Figure 5. Left: The near-infrared spectrum of Mars between 2 and 5 μm, recorded by the Short Wavelength Spectrometer of the Infrared Space Observatory (Lellouch et al. 2000). The spectrum is largely dominated by CO_2, with very minor contributions from H_2O and CO. Right: Examples of thermal spectra of Mars recorded by the IRIS spectrometer aboard Mariner 9 (Hanel et al. 2003). The upper spectrum is recorded in the equatorial region, where the surface is warmer than the atmosphere. The lower spectrum is recorded in a polar region, where the polar cap is colder than the atmosphere. Note the absorption core in the CO_2 emission band, which illustrates that the atmospheric temperature decreases as the altitude increases.

temperature where the optical depth is equal to 1 (or 2/3 if we consider the disk-integrated outgoing flux). As a result, the thermal spectrum of a planet may exhibit emission or absorption lines, depending on the temperature gradient of the emitting region. The lines will be in absorption if they are formed in the troposphere, where the gradient is negative; they will appear in emission if they are formed in the stratosphere where the temperature increases with the altitude (Encrenaz & Lequeux 2022).

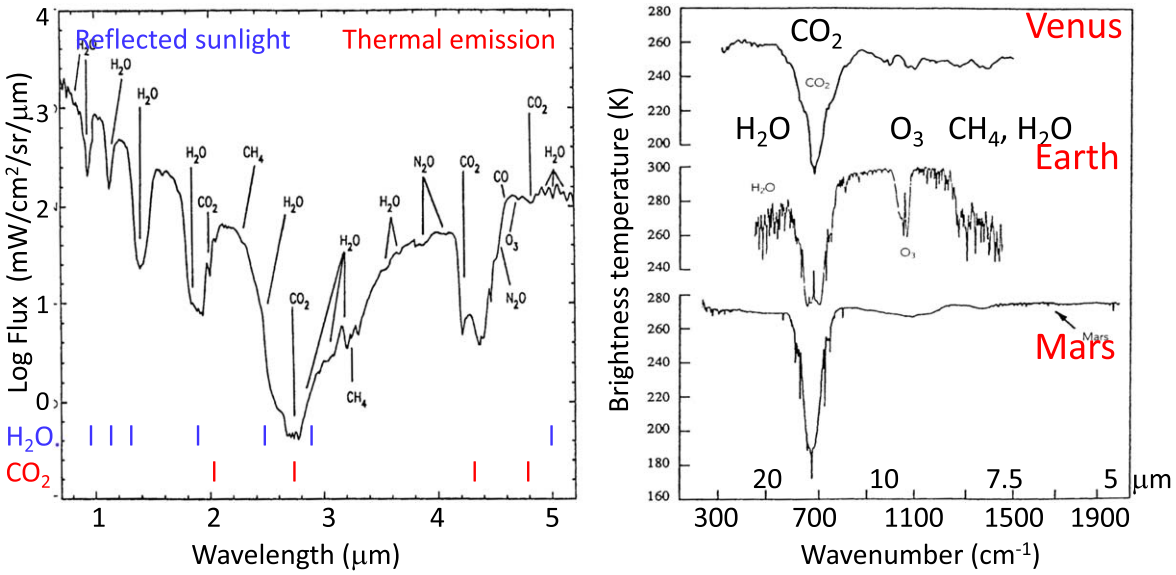

Figure 6. Left: Near-infrared spectrum of the Earth, recorded by the NIMS-Galileo instrument during its Earth flyby in 1990 December (Drossart et al. 1993). The flux scale is logarithmic. The spectrum is dominated by H_2O and CO_2, with contributions from CO, CH_4 and N_2O. Right: Thermal spectra of Venus, Mars and the Earth recorded by in-orbit FT spectroscopy (Hanel et al. 2003). The ordinate unit is the brightness temperature; it corresponds to the cloud temperature in the case of Venus, and to the surface temperature in the case of the Earth and Mars. The strong CO_2 band at 15 μm appears on the 3 planets. The signature of ozone O_3 near 10 μm is clearly visible on the Earth spectrum.

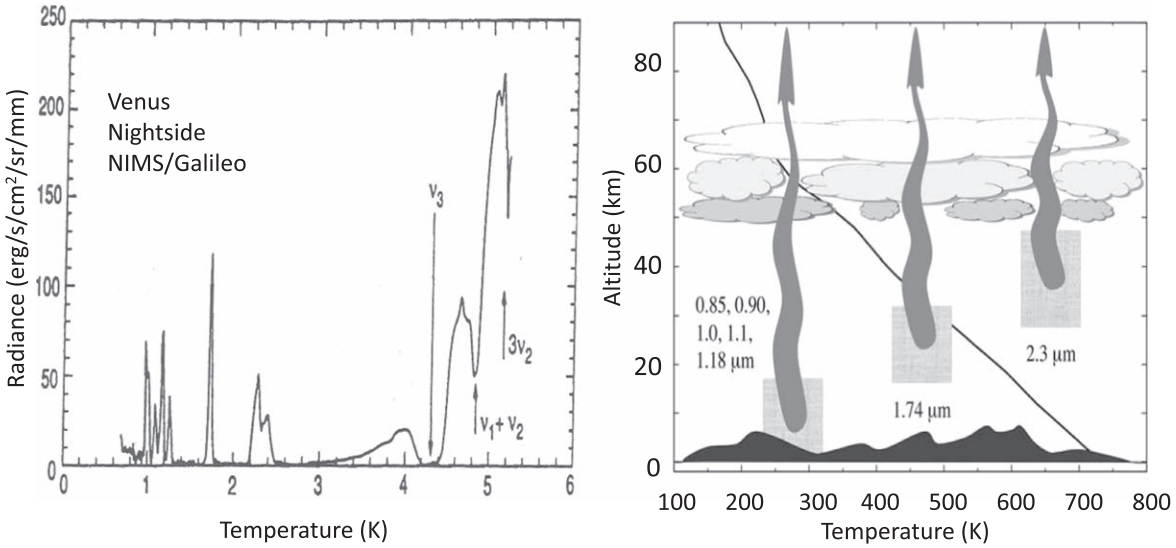

Figure 7. Left: The nightside spectrum of Venus between 0.8 and 5.3 μm, recorded by the NIMS spectrometer aboard the Galileo spacecraft during its flyby of Venus in 1990 February. The flux coming from the surface and/or the lower troposphere is detected between the strong bands of CO_2 (Carlson et al. 1991). Right: Penetration level of the flux at various wavelengths (Bézard & de Bergh 2007). The 2.7 μm window probes the lower atmosphere at an altitude of about 30 km, while around 1 μm, the radiation comes from the few kilometers above the surface.

Figures 5–9 show examples of near-infrared spectra of terrestrial planets. In all cases, the two components, reflected and thermal, are easily identified at short wavelengths and long wavelengths respectively. In the case of Venus and Mars, the spectra are dominated by carbon dioxide, the main atmospheric component, which is also a very efficient spectroscopic agent. The situation is different in the case of the Earth, which has a spectrum dominated by H_2O and CO_2, two very minor components. The reason is that the two main atmospheric constituents, molecular nitrogen and molecular oxygen, are not

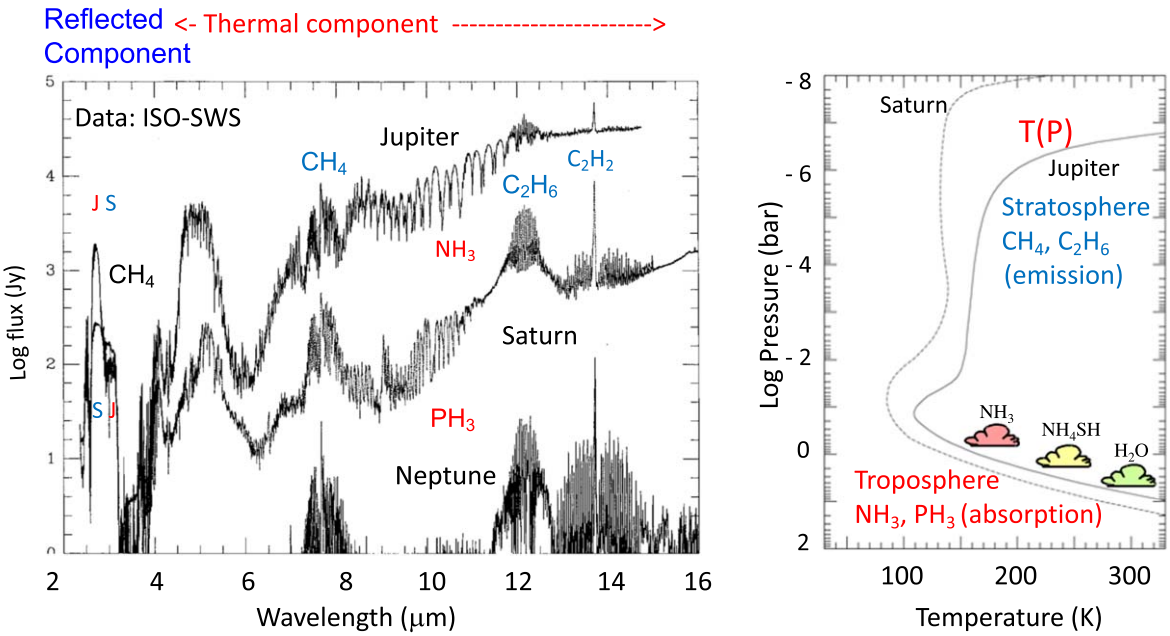

Figure 8. Left: The spectrum of the giant planets between 2 and 16 μm, recorded by the Short Wavelength Spectrometer of the Infrared Space Observatory (Encrenaz et al. 1999). Right: A schematic view of the thermal profiles of Jupiter and Saturn illustrating where the radiation originates. In the thermal regime, emission bands are formed in the stratosphere, while absorption features are formed in the troposphere.

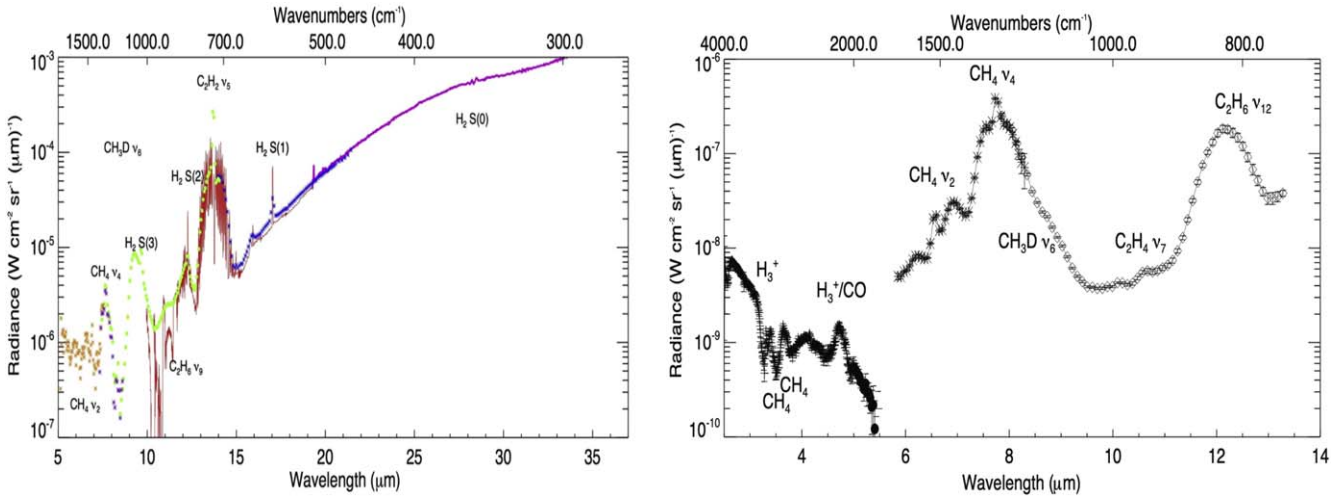

Figure 9. Left: The spectrum of Uranus between 5 and 35 μm, as observed by the different modules of the infrared spectrometer aboard the Spitzer observatory (Orton et al. 2014). Right: The spectrum of Neptune between 3.0 and 13.5 μm, recorded by the IRC spectrometer of the Akari observatory (Fletcher et al. 2010). In addition to H_2 and hydrocarbon signatures, the spectrum of Neptune shows emission lines of CO formed by fluorescence in the upper stratosphere (see text).

spectroscopically active. This actually explains why the greenhouse effect is moderate on Earth, while it is very strong on Venus (in the case of Mars, the greenhouse effect is very limited because the surface pressure is less than 0.01 bar). In the case of Mars (Figure 5), the spectrum is typical of a very thin, CO_2-dominated atmosphere. The thermal spectra illustrate that, depending on the surface temperature, the CO_2 emission at 15 μm may appear in absorption (when the surface is warmer than the atmosphere, at mid-latitudes) or in emission (at the poles, when the surface is colder than the atmosphere). The spectrum of the Earth (Figure 6) is mostly dominated by H_2O and CO_2. Although the partial pressures of these species are less than 1%, they are the most important spectroscopic agents. An important feature is the signature of ozone O_3 near 10 μm, well separated from other atmospheric features. This signature appears as a key potential diagnostic in the search for life on

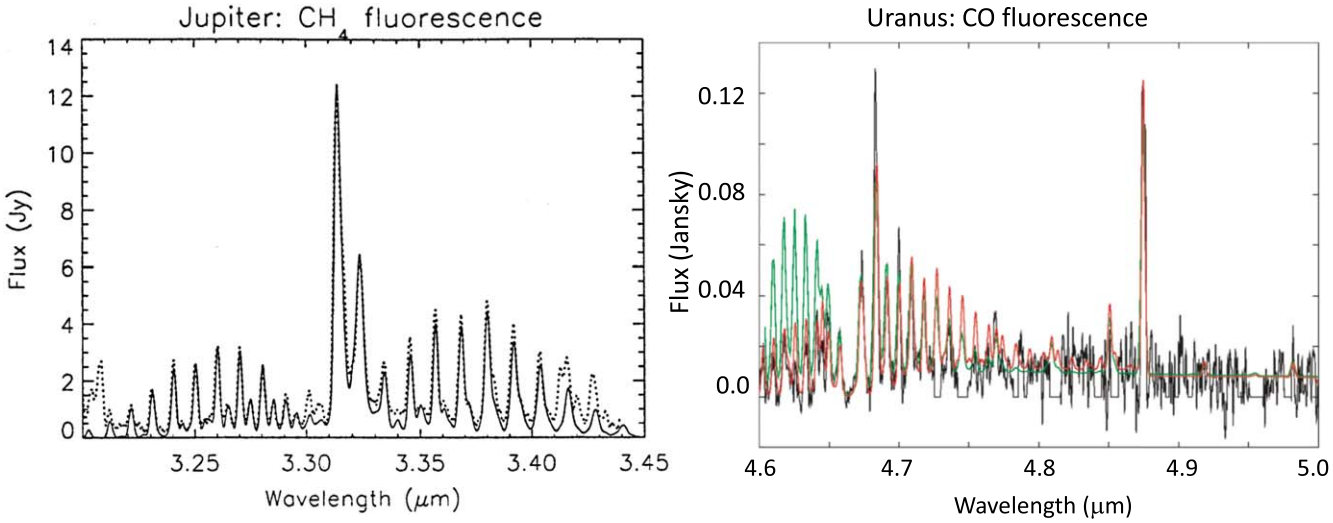

Figure 10. Left: Fluorescence emission of methane in Jupiter near 3.3 μm. This observation was used for an estimate of the eddy diffusion coefficient at the homopause (Drossart et al. 1999). Right: Fluorescence emission of CO in Uranus, observed with the ISAAC imaging spectrometer of the Very Large Telescope (ESO, Chile). Black line: data. Green line: Synthetic spectrum calculated with a radiative transfer code using the Local Thermodynamical Equilibrium (LTE) assumption. Red curve: Synthetic spectrum calculated with a non-LTE fluorescence model (Encrenaz et al. 2004).

rocky exoplanets. The near-infrared spectrum of Venus (Figure 7) shows an interesting distinctive feature. Because the surface temperature of Venus is very high (730 K), its thermal emission is high enough to be detected on the night side of the planet, in a few spectral windows (around 1.0 μm, and at 1.7 and 2.3 μm), between the strong CO_2 absorption bands (Taylor 2014). Apart from the radar range, this is actually the only spectral range where the lower troposphere and the surface of Venus can be probed remotely. Unfortunately, such situation is unlikely to be observed on exoplanets because the transit spectroscopy technique, which is presently the best method for probing exoplanetary atmospheres, does not probe below the clouds of the planet, as will be discussed below.

Figure 8 depicts the infrared spectra of Jupiter and Saturn between 2 and 16 μm, both in the reflected and thermal regimes. Although both giant planets might look more or less similar at first glance, it is striking to notice how the spectra are different. Both spectra feature a spectral window around 5 μm which probes the lower troposphere. Stratospheric emissions of CH_4, C_2H_6 and C_2H_2 are present on both planets, but, in the troposphere, NH_3 dominates the Jovian spectrum while Saturn's one is dominated by PH_3. There are two reasons for these differences: (1) Because Saturn is colder, there is less gaseous NH_3 in its atmosphere; (2) Vertical mixing, as described above, is more active on Saturn than on Jupiter, and the PH_3 abundance is consequently larger. This simple example illustrates that, in the case of giant exoplanets, we can be prepared for a large variety of thermal spectra. We also have to remember that knowing the thermal profile is essential for a proper interpretation of these spectra.

Figure 9 shows the infrared disk-integrated spectra of Uranus and Neptune as observed by the Spitzer and Akari observatories, respectively (Fletcher et al. 2010; Orton et al. 2014). In both cases, the reflected component extends up to 6 μm. The spectra are dominated by stratospheric emission signatures due to hydrogen, methane and hydrocarbons. All tropospheric species detected in Jupiter and Saturn (NH_3, PH_3, GeH_4, ...) are in condensed form and thus undetectable. An exception is H_2S, tentatively identified in both planets in the reflected part around 3 μm. Hydrogen sulfide is expected to condense on both planets at a level of a few bars and a temperature of about 120 K (de Pater et al. 1991). In the mid-infrared range, the brightest emission feature is the ν_5 band of C_2H_2 at 13.7 μm, as also displayed in Figure 8.

In addition to the reflected sunlight component and the thermal component, another spectral signature may be present in infrared spectra of solar system planets. Fluorescence emission appears when a solar photon is absorbed by a molecule (or an atom or a radical). It can be re-emitted at the same wavelength (resonant fluorescence) or in a cascade at longer wavelengths. This mechanism is mostly observed in cometary atmospheres, in the ultraviolet (UV), visible and near-infrared spectral ranges (Wilkening & Matthews 1982; Crovisier & Encrenaz 1983). It has also been observed in the stratospheres of the giant planets in a few cases (Figure 10). In particular, resonant fluorescence of methane has been observed at 3.3 μm in the upper stratosphere of Jupiter and Saturn (Drossart et al. 1999); resonant fluorescence of CO has been observed on terrestrial planets (Gilli et al. 2011; Marcq et al. 2015), Uranus (Encrenaz et al. 2004), Neptune (Fletcher et al. 2010, Figure

10) and Titan (Lellouch et al. 2003) at 4.7 μm. This mechanism has to be mentioned as it could take place in the upper atmospheres of exoplanets. Indeed, resonant fluorescence of CH_4 at 3.3 μm has been reported from ground-based spectroscopic measurements of the hot Jupiter HD 189733 b (Swain et al. 2010; Waldmann et al. 2012).

4. Transit Spectroscopy of Solar System Planets

Most of our knowledge regarding the atmospheric composition of exoplanets comes from the visible and infrared spectroscopy of transiting exoplanets. With the advent of James Webb Space Telescope (JWST), this field of research is expected to develop even more in the future. In parallel, near-infrared spectroscopy of young giant exoplanets, detected by imaging techniques is also expected to grow in the near future. Both methods are complementary: while primary transit spectroscopy probes by transmission through the upper atmosphere of the planet at terminator, the spectroscopy of exoplanets observed by imaging gives the emission spectrum of the exoplanet; in the same way, the secondary transit spectroscopy gives the emission spectrum of the exoplanet on the dayside (Tinetti et al. 2013). In the latter case, the disk-integrated infrared spectra of solar system planets provide us with analogs of the spectra we can expect for exoplanets. In contrast, we have no analog of transmission spectra of solar system planets, with the only exception being the spectroscopy of Venus recorded during transits of Venus in front of the Sun (Tanga et al. 2012). In this section, we address the following question: What could we learn from transit observations of solar system planets?

Let us consider an observer located in the ecliptic plane at some distance from the solar system, for instance on 29 Arietis (29 Ari), a star located at 30 pc, with an ecliptic latitude of $+0\overset{\circ}{.}018$. The observer would see the Earth transiting around the Sun. Would the other planets transit also? The answer is no, because of two reasons: (1) the inclinations of the planets' orbits are higher than 1°, except for Uranus which has an inclination of $0\overset{\circ}{.}8$; (2) as compared to exoplanetary systems, all planets are very far from the Sun. Mercury, the closest planet from the Sun, is located at about 80 solar radii. By comparison, 51 Peg b is located at 6 stellar radii from its host star. An analog is provided by the Jovian system of Galilean satellites: Io is located at 6 Jovian radii from the planet and Callisto at 25 radii; this configuration allows multiple transit and occultation phenomena.

As seen from a point located in the ecliptic plane, a planet will transit in front of the Sun if its angular distance to the ecliptic is smaller than $\alpha = R_{\rm Sun}/D$, with $R_{\rm Sun}$ being the solar radius and D the heliocentric distance of the planet. This distance varies from $0\overset{\circ}{.}7$ in the case of Mercury to $0\overset{\circ}{.}18$ in the case of Mars, and from $0\overset{\circ}{.}052$ in the case of Jupiter to less than $0\overset{\circ}{.}001$ in the case of Neptune. For a planet to transit regularly around the Sun, this angle has to be smaller than the inclination i of its orbit on the ecliptic. As shown in Table 1, these values are far smaller than the inclinations of the planetary orbits with respect to the ecliptic plane which means that no regular transit can be observed for any of the planets; as observed from a random point in the ecliptic, the solar system would be seen as a single planetary system.

Table 1
Observability of Planetary Transits from a Point in the Ecliptic Plane

Planet	D (au)	α (degree)	i (degree)	Long. of asc. Node	Long. on 2020 May 1
Mercury	0.4	0.7	7	48.33	21
Venus	0.7	0.4	3.4	71.68	198
Earth	1.0	0.27	0	⋯	220
Mars	1.5	0.18	1.8	49.55	278
Jupiter	5.2	0.052	1.3	100.46	286
Saturn	9.5	0.028	2.5	113.66	296
Uranus	19.2	0.014	0.8	74 .01	36
Neptune	30.1	0.0009	1.8	131.78	349

Figure 11 illustrates a view of the solar system as seen from the north ecliptic pole. For simplicity, the orbits of the planets are assumed to be circular. The node lines show, for each planet, the intersection of its orbital plane with the ecliptic. An observer located on one of these node lines would see the solar system as a 2-planet transiting system, with two exceptions. We note that the ecliptic longitudes Ω of Mars and Mercury are separated by only $\Delta\Omega = 1\overset{\circ}{.}22$ (Table 1). For an observer located on the node line of Mars, the closest angular distance of Mercury to the Sun is equal to b, such that

$$\sin b = \sin \Delta\Omega \times \sin i$$

where i is the inclination of the orbit of Mercury over the ecliptic. As the angles are very small, this equation becomes

$$b = \Delta\Omega \times i \times \pi/180 = 0\overset{\circ}{.}15$$

which is less than the α value for Mercury ($0\overset{\circ}{.}7$, see Table 1). In the same way, the longitudes of the node lines of Venus and Uranus are separated by only $2\overset{\circ}{.}33$ (Table 1). In this case, the closest angular distance of Venus to the Sun, as seen from the node line of Uranus, is $b = 0\overset{\circ}{.}14$, which is smaller than the α value of Venus ($0\overset{\circ}{.}4$). In conclusion, along the node lines of Mars and Uranus, the solar system appears as a 3-planet transiting system. It will be the case if $\Delta\Omega$ is smaller than 5° near the Mars node line, and 6° near the Uranus node line. Thus, a 3-planet transit will be observed for longitudes between 45° and 53°, and between 68° and 77° (note that the precession of the nodes is not taken into account in this calculation).

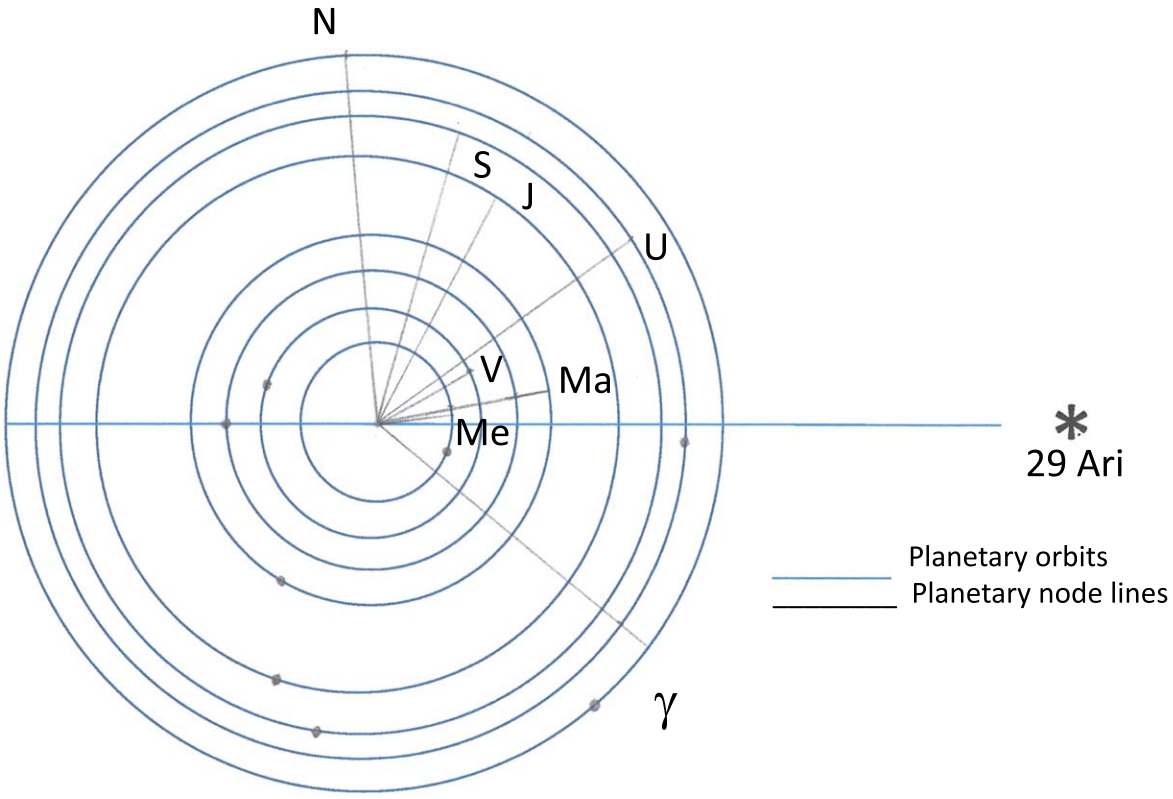

Figure 11. A simplified view of the solar system as observed from the north ecliptic pole. The Sun is at the center of the figure and the horizontal axis points toward the direction of 29 Ari. The orbits of the planets are assumed to be circular, and their radii are not to scale. The blue lines are the node lines of the planets, i.e., the intersection of their orbital plane with the ecliptic. The black points correspond to the positions of the planets on 2020 May 1. This date corresponds to a secondary transit of the Earth as seen from a point on the *X*-axis (close to the location of the star 29 Ari).

4.1. The Lightcurve of the Solar System

As the solar system planets are all close to the ecliptic plane, even in the absence of transits, the light curve of the solar system, as seen from the ecliptic plane, is expected to bear the signatures of the planets. In this section, we estimate the contributions of the primary transit and the secondary transit of each planet at two different wavelengths, in the visible range (reflected solar radiation) and at 10 μm (thermal emission). In the case of solar system planets, the thermal emission of the planet is negligible in the visible range (it would not be the case for a hot Jupiter, as shown in Figure 4).

The amplitude of the primary transit, in both the solar reflected and thermal components, is given by

$$A_p = [R_{\rm plan}/R_{\rm sol}]^2$$

where $R_{\rm plan}$ and $R_{\rm sol}$ are the planetary and solar radii, respectively.

The amplitude of the secondary transit, in the solar reflected component, is given by

$$A_s = [R_{\rm plan}/D_{\rm plan}]^2 \times a$$

where $D_{\rm plan}$ is the distance of the planet to the Sun and a is the albedo.

At 10 μm (thermal regime), the amplitude of the secondary transit is expressed as

$$\rho = [R_{\rm plan}/R_{\rm sol}]^2 \times {\rm BB}(T_{\rm day})/{\rm BB}(T_{\rm sol})$$

where ${\rm BB}(T_{\rm day})$ and ${\rm BB}(T_{\rm sol})$ are the blackbodies corresponding to the solar temperature and the planetary dayside temperature, respectively.

The transit time t of a planet is written

$$t = P \times 2R_{\rm sol}/[2\pi D]$$

where P is the revolution period of the planet and D its distance to the Sun.

Results are summarized in Table 2, and shown in Figures 12 and 13. In Table 2, a is the albedo, A_p is the primary transit absorption (solar reflected light and thermal regimes) and A_s is the secondary transit absorption (solar reflected light). $T_{\rm day}$ and $T_{\rm night}$ are the dayside and nightside temperatures (at the surface or, in the case of Venus and the giant planets, at the cloud top) respectively, ρ_s is the thermal absorption at secondary transit and ρ_p is the thermal absorption at primary transit.

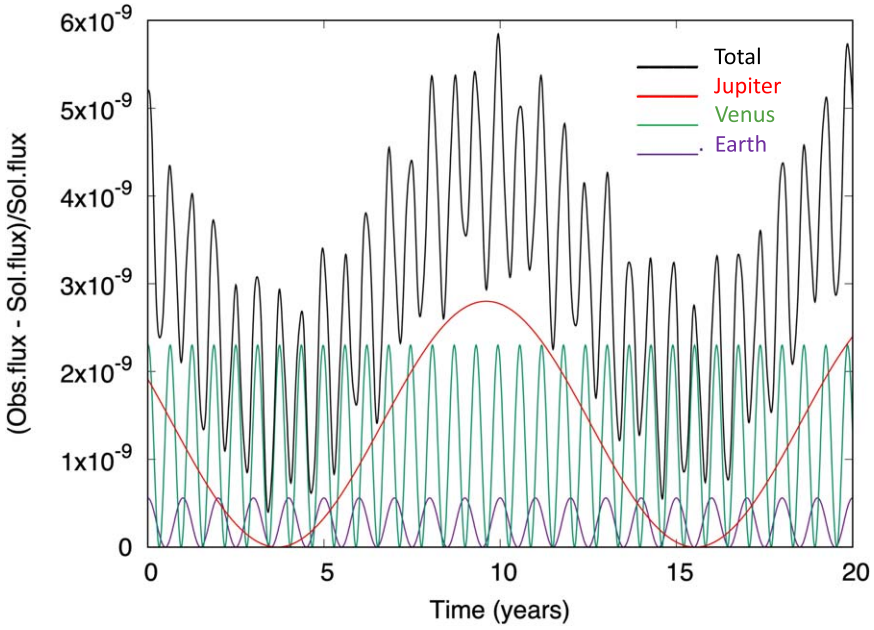

Figure 12. A simplified version of the lightcurve of the solar system in the visible range (solar reflected component). The contribution of each planet is represented by a sinusoid with a maximum value at secondary transit (full dayside planetary disk observed) and minimum value at primary transit (no contribution from the nightside). The origin of the abscissa axis is 2020 May 1. Black line: Total; red line: Jupiter; green line: Venus; blue line: Earth. The main contributions come from Jupiter, Venus and the Earth, followed by Saturn and Mercury (see Table 1).

Table 2
The Solar System as Seen in Transit: Inputs and Results

Planet	a	A_p	A_s	$T_{\rm day}$	$T_{\rm night}$	ρ_s	ρ_p	t (hr)
Mercury	0.12	1.2×10^{-5}	2.1×10^{-10}	700	90	5.0×10^{-7}	$3.7 \times 10 - 13$	8.0
Venus	0.75	7.5×10^{-5}	2.3×10^{-9}	235	235	4.7×10^{-8}	4.7×10^{-8}	11.1
Earth	0.31	8.4×10^{-5}	5.6×10^{-10}	288	278	1.6×10^{-7}	1.3×10^{-7}	12.9
Mars	0.25	2.3×10^{-5}	5.5×10^{-11}	250	180	2.1×10^{-8}	2.2×10^{-9}	16.0
Jupiter	0.34	1.0×10^{-2}	2.9×10^{-9}	124	124	2.7×10^{-8}	2.7×10^{-8}	29.4
Saturn	0.34	7.5×10^{-3}	6.0×10^{-10}	95	95	5.5×10^{-10}	5.5×10^{-10}	39.8
Uranus	0.30	1.3×10^{-3}	2.3×10^{-11}	58	58	6.3×10^{-15}	6.3×10^{-15}	56.3
Neptune	0.29	1.3×10^{-3}	8.8×10^{-12}	58	58	5.9×10^{-15}	5.9×10^{-15}	70.1

The main conclusion is that, because the solar system planets are relatively far from the Sun, the contribution of the planets to the solar system lightcurve is very small, too small to be detectable by any present observational means. In the visible range, the main contribution comes from Jupiter, followed by the ones by Venus and the Earth. In the thermal range, the amplitude of the modulation depends upon the difference between the daytime temperature and the nighttime temperature; it is thus zero for Venus and the giant planets (Table 1). The contribution of Mercury prevails, due to its high dayside surface temperature and low nightside temperature. In any case, the overall modulation of the solar system lightcurve is below 10^{-8} in the visible range and 10^{-6} at 10 μm. As displayed in Table 1, the time transits for the planets are in the range of 8–16 hr for the terrestrial planets, and 30–70 hr for the giant planets. Assuming a typical atmospheric height of 100 km, the transit time for the atmosphere during primary transit would be 2–4 s for the terrestrial planets, and 7–16 s for the giant planets.

4.2. Primary Transit Spectra of the Solar System Planets

In this section, we calculate synthetic primary transit spectra of solar system planets in the infrared range. Our objective is to identify the information which could be retrieved from this kind observation when it becomes available for giant and super-Earth exoplanets, and to compare the relative merits of primary transit spectroscopy with respect to secondary spectroscopy (i.e., disk-integrated dayside emission spectroscopy). Similar calculations have been performed by Irwin et al. (2014) in the case of the Earth and Jupiter.

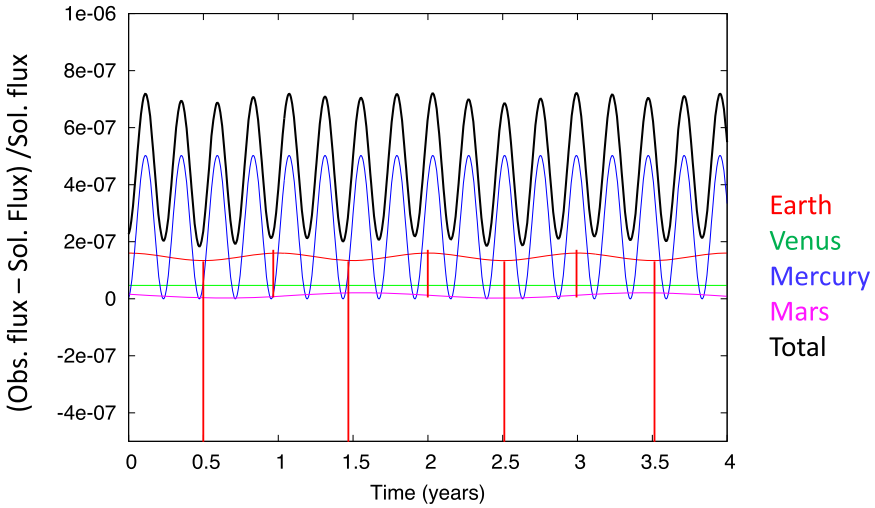

Figure 13. The lightcurve of the inner solar system in the thermal range (10 μm). The contribution of each planet is represented by a sinusoid with a maximum value at secondary transit (blackbody at dayside temperature) and minimum value at primary transit (blackbody at nightside temperature). The origin of the abscissa axis is 2020 May 1. Black line: total; blue line: Mercury; green line: Venus; red line: Earth; purple line: Mars. The main contribution comes from Mercury, which has a maximum dayside/nightside temperature contrast. The modulation due to the giant planets is zero because their dayside and nightside temperature are equal. The primary and secondary transits of the Earth are indicated by red vertical lines. The contribution of Jupiter (not shown in the figure) would be half that of Venus (Table 1).

In a primary transit, the amplitude of the atmospheric absorption $A_{\rm atm}$ (i.e., the annulus due to the atmosphere around the solid planetary body) can be estimated by the following equation (Perryman 2011; Tinetti et al. 2013)

$$A_{\rm atm} = 5 \times [2R_P H/R_{\rm sol}^2]$$

where H is the scale height

$$H = RT/\mu g$$

with R being the perfect gas constant, T the temperature, μ the mean molecular weight of the atmosphere and g the gravity.

In the case of hot Jupiters, typical values of $A_{\rm atm}$ are around 100 ppm. In the case of solar system planets, lower values can be expected because their atmospheric temperatures are lower. Table 3 gives the values of $A_{\rm atm}$ for the solar system planets.

Our tool for generating the synthetic planetary spectra is the Planetary Spectrum Generator (PSG) developed by G. Villanueva and his team at the NASA Goddard Space Flight Center (Villanueva et al. 2018). This very powerful tool is an online radiative transfer suite that can synthesize planetary spectra at any spectral resolution in a wide range of wavelengths from the UV to the radio range, by combining several state-of-the-art radiative transfer models, spectroscopic databases and planetary databases. PSG can synthesize spectra for any observer and target configuration, including nadir, limb and solar/stellar occultation (Villanueva et al. 2018). Template atmospheric models are defined on the basis of recent observations (Robinson & Catling 2014).

Figure 14 depicts primary transit infrared spectra of the Earth, Mars, Jupiter, Saturn, Uranus and Neptune as calculated with the PSG, between 2 and 17 μm, with a spectral resolving power of 200. These characteristics are chosen to prepare a comparison with JWST spectra, to be recorded in the near future (Beichman & Greene 2018). The first comment to be made is that, in all cases, the upper atmosphere is probed, i.e., the stratosphere in the case of the Earth and the giant planets, and the mesosphere in the case of Venus. In the terrestrial atmosphere, the presence of H_2O, CO_2 and O_3 above the clouds would be recognized. In the case of Venus, CO_2 and SO_2 would be identified above the clouds. In the case of the giant planets, CH_4 and its photodissociation products would be identified. As in the case of Jupiter and Saturn, the spectra of Uranus and Neptune are dominated by CH_4, C_2H_2 and C_2H_6.

We can use Figure 14, as well as Figures 5–9, to discuss the relative merits of primary transit spectroscopy and secondary transit spectroscopy to infer the properties of planetary atmospheres. Primary transit spectroscopy appears to be very

Table 3
Amplitude of the Atmospheric Absorption $A_{\rm atm}$ of the Solar System Planets as seen in Primary Transit

Planet	g (m s^{-2})	μ (g mol^{-1})	H (km)	$A_{\rm atm}$ (ppm)
Venus	8.9	44	5.0	0.6
Earth	9.8	29	8.5	1.0
Mars	3.7	44	11.1	0.7
Jupiter	24.8	2.2	22	30
Saturn	10.4	2.2	36.3	40
Uranus	8.9	2.6	18.1	8
Neptune	11.1	2.6	14.5	7

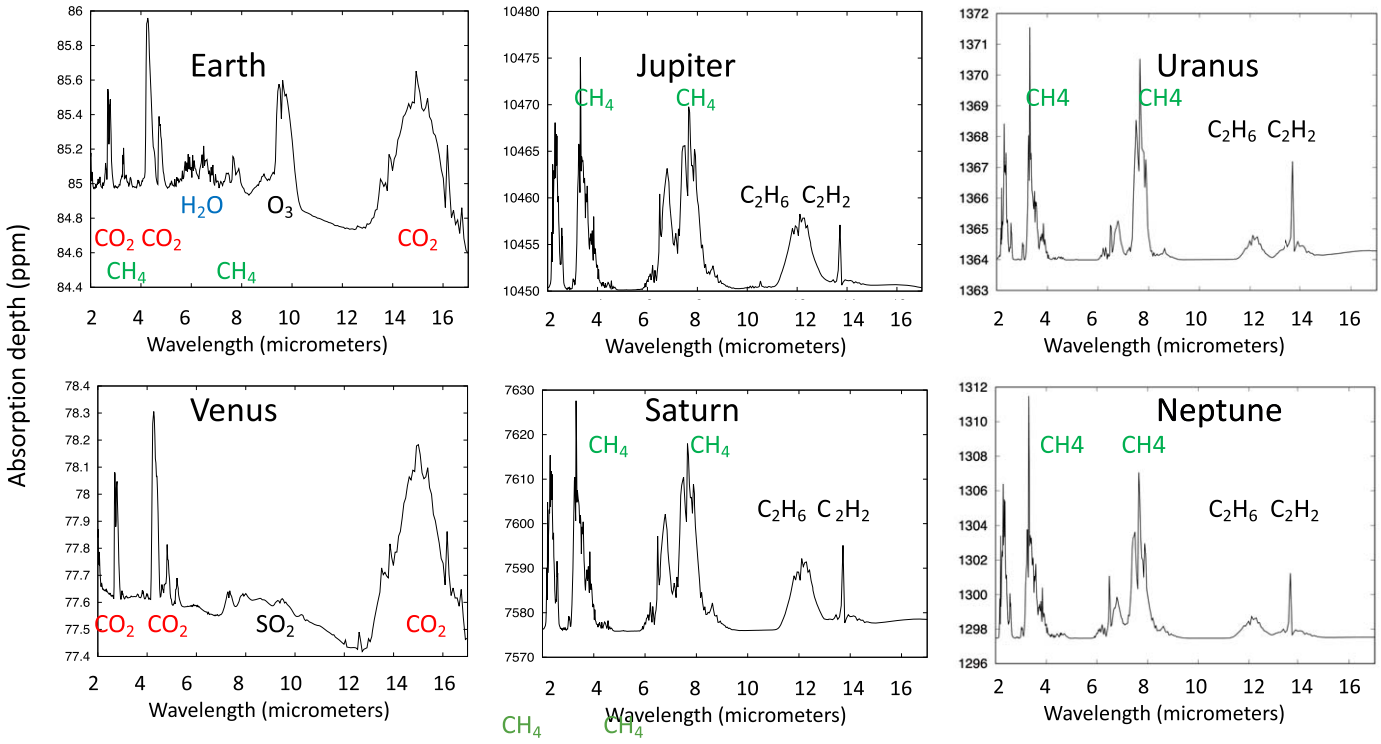

Figure 14. Synthetic primary transit infrared spectra of solar system planets, calculated with the PSG (Villanueva et al. 2018), with a resolving power of 200. Top left: Earth; Bottom left: Venus. Top middle: Jupiter; bottom middle Saturn. Top right: Uranus; Bottom right: Neptune.

sensitive for probing the upper atmospheres. Indeed, the solar occultation technique has been successfully used to probe the upper atmospheres of Mars and Venus from orbital measurements aboard Mars Express (Bertaux 2006), Trace Gas Orbiter (Vandaele et al. 2018) and Venus Express (Vandaele et al. 2016). The method is still being applied with great success in the case of Mars.

When conducting limb observations, the number of molecules along the line of sight is much larger than the number of molecules seen in the nadir geometry. The amplifying factor is given by the Chapman factor C

$$C = \sqrt{(2\pi R/H)^{0.5}}$$

where R is the planetary radius and H its scale height. For an Earth-like planet, C is as high as 70 at the surface; in practice, limb observations are limited to stratospheric or mesospheric observations because of the presence of clouds or aerosols. In the case of a hot Jupiter, C is equal to about 10.

For secondary transits, observing the entire planetary disk increases the air mass, and hence the sensitivity for detecting minor species, by a factor of about 4, but primary transit spectroscopy remains more sensitive. The limitation is that, in all cases, no information can be retrieved below the clouds about the tropospheric composition. In particular, in the case of Venus, primary transit spectroscopy would not allow the determination of the high temperature and pressure at the surface (note that the full disk-integrated emission spectrum of Venus would not provide this information either; specific observations of the night side of Venus at specific near-infrared wavelengths would allow it, as shown in Figure 7). It thus appears that both primary and secondary transit spectroscopy are complementary. Direct emission spectroscopy is important for probing the whole atmosphere; such observations are expected to develop in the near future for exoplanets observed by direct imaging; this is the case, in particular for the exoplanet PDS 70 b (Mueller et al. 2018).

5. Conclusions

In this paper, we have tried to show that many lessons can be retrieved from our knowledge of the solar system to better characterize the nature and atmospheric properties of exoplanets. Over the past twenty years, a permanent synergy has developed between solar system planetology and the exploration of exoplanets.

In the field of planetary formation modeling, the old model of the protosolar nebula, first proposed by Kant and Laplace over two centuries ago, has proved to be appropriate, at least in its general baseline, for many exoplanetary systems. Protoplanetary disks, including gaps revealing possible evidence for exoplanet formation, can now be directly imaged in the radio

range thanks to the capability of the Atacama Large Millimeter/submillimeter Array network of antennas (Andrews et al. 2016).

Inversely, the discovery of the migration process as a major mechanism at work in exoplanetary systems has boosted the development of numerical simulations of the dynamical evolution of solar system objects with, in particular, the major influence of the giant planet migration in the past history of the solar system (Tsiganis et al. 2005; Walsh et al. 2011).

As the chemical atmospheric composition of an increasing number of exoplanets is being revealed, thanks mostly to the spectroscopy of transiting exoplanets, radiative transfer models, adapted from solar system studies, have been successfully applied to constrain the temperature and cloud structures of these exoplanetary atmospheres. This also applies to Global Climate Models, initially developed to understand the meteorology and climate of the Earth. After being successfully adapted to all solar system planets (Forget et al. 1999; Forget & Lebonnois 2013), they are now used for predicting what could be the stability and climate of an exoplanet's atmosphere with, in some cases, exotic orbital and physical properties (Forget & Leconte 2014; Charnay et al. 2015; Heng & Showman 2015; Turbet et al. 2016).

In the near future, the advent of JWST, especially with its infrared spectrometers NIRSpec and MIRI, is expected to provide us with a new major step in our exploration of exoplanetary atmospheres (Beichman & Greene 2018). Within a few years, the Ariel space mission of ESA is expected to deliver infrared spectra of a thousand exoplanets exhibiting all orbital and physical properties, allowing us to better characterize these new worlds (Tinetti et al. 2018).

Acknowledgments

This work was funded by Paris Observatory and the Centre National de la Recherche Scientifique. I am grateful to Giovanna Tinetti for having introduced me to the new field of exoplanet spectroscopy. I am grateful to Wing Ip, Françoise Roques, Athena Coustenis, Gabriella Gilli and Emmanuel Marcq for helpful discussions regarding this paper.

References

Andrews, S. M., Wilner, D. J., Zhu, Z., et al. 2016, ApJL, 820, L40
Beaulieu, J. -P., Bennett, D. P., Fouqué, P., et al. 2006, Natur, 439, 437
Beichman, C. A., & Greene, T. P. 2018, arXiv:1803.03730
Bertaux, J. -L. 2006, JGRE, 111, E09S01
Bézard, B., & de Bergh, C. 2007, JGRE, 112, E04S07
Cameron, A. G. W. 1988, ARA&A, 26, 441
Carlson, R. W., Baines, K. H., Encrenaz, T., et al. 1991, Sci, 253, 1541
Charbonneau, D., Brown, T. M., Latham, D. W., et al. 2000, ApJL, 529, L45
Charnay, B., Meadows, V., Misra, A., et al. 2015, ApJL, 813, L1
Chauvin, G., Lagrange, A. -M., Zuckerman, B., et al. 2005, A&A, 438, L29
Crovisier, J., & Encrenaz, T. 1983, A&A, 126, 170
de Pater, I., Romani, P. N., & Atreya, S. K. 1991, Icar, 91, 220
Drossart, P., Fouchet, T., Crovisier, J., et al. 1999, The Universe as Seen by ISO, 427, 169
Drossart, P., Rosenqvist, J., Encrenaz, T., et al. 1993, P&SS, 41, 551
Encrenaz, T., Drossart, P., Feuchtgruber, H., et al. 1999, P&SS, 47, 1225
Encrenaz, T., Lellouch, E., Drossart, P., et al. 2004, A&A, 413, L5
Encrenaz, T., & Lequeux, J. 2022, The Solar System. ISTE Editions
Feuchtgruber, H., Lellouch, E., de Graauw, T., et al. 1997, Natur, 389, 159
Fletcher, L. N., Drossart, P., Burgdorf, M., et al. 2010, A&A, 514, A17
Forget, F., Hourdin, F., Fournier, R., et al. 1999, JGR, 104, 24155
Forget, F., & Lebonnois, S. 2013, Comparative Climatology of Terrestrial Planets (Tucson, AZ: Univ. Arizona Press), 213
Forget, F., & Leconte, J. 2014, RSPTA, 372, 20130084
Fulton, B. J., Petigura, E. A., Howard, A. W., et al. 2017, AJ, 154, 109
Gilli, G., López-Valverde, M. A., Funke, B., et al. 2011, P&SS, 59, 1010
Hanel, R. A., Conrath, B. J., Jennings, D. E., et al. 2003, in Exploration of the Solar System by Infrared Remote Sensing, ed. R. A. Hanel et al. (Cambridge: Cambridge Univ. Press), 534
Heng, K., & Showman, A. P. 2015, AREPS, 43, 509
Irwin, P. G. J., Barstow, J. K., Bowles, N. E., et al. 2014, Icar, 242, 172
Lellouch, E., Coustenis, A., Sebag, B., et al. 2003, Icar, 162, 125
Lellouch, E., Encrenaz, T., de Graauw, T., et al. 2000, P&SS, 48, 1393
Lewis, J. S. 1995, Physics and Chemistry of the Solar System (San Diego, CA: Academic)
Lissauer, J. J., & de Pater, I. (ed.) 2013, Fundamental Planetary Science (Cambridge: Cambridge Univ. Press)
Marcq, E., Lellouch, E., Encrenaz, T., et al. 2015, P&SS, 113, 256
Mayor, M., & Queloz, D. 1995, Natur, 378, 355
Mizuno, H. 1980, PThPh, 64, 544
Morbidelli, A., Baillié, K., Batygin, K., et al. 2022, NatAs, 6, 72
Müller, A., Keppler, M., Henning, T., et al. 2018, A&A, 617, L2
Orton, G. S., Fletcher, L. N., Moses, J. I., et al. 2014, Icar, 243, 494
Perryman, M. 2011, The Exoplanet Handbook by Michael Perryman (1 ed.; Cambridge: Cambridge Univ. Press), 424
Pollack, J. B., Hubickyj, O., Bodenheimer, P., et al. 1996, Icar, 124, 62
Robinson, T. D., & Catling, D. C. 2014, NatGe, 7, 12
Swain, M. R., Deroo, P., Griffith, C. A., et al. 2010, Natur, 463, 637
Tanga, P., Widemann, T., Ambastha, A., et al. 2012, AAS/Division for Planetary Sciences Meeting Abstracts, 44, 508.07
Taylor, F. W. (ed.) 2014, The Scientific Exploration of Venus (Cambridge: Cambridge Univ. Press)
Tinetti, G., Drossart, P., Eccleston, P., et al. 2018, ExA, 46, 135
Tinetti, G., Encrenaz, T., & Coustenis, A. 2013, A&ARv, 21, 63
Trilling, D. E., Lunine, J. I., & Benz, W. 2002, A&A, 394, 241
Tsiganis, K., Gomes, R., Morbidelli, A., et al. 2005, Natur, 435, 459
Turbet, M., Leconte, J., Selsis, F., et al. 2016, A&A, 596, A112
Vandaele, A. C., Lopez-Moreno, J. -J., Patel, M. R., et al. 2018, SSRv, 214, 80
Vandaele, A. C., Neefs, E., Ristic, B., et al. 2016, AAS/DPS Meeting Abstracts, 48, 404.07
Villanueva, G. L., Smith, M. D., Protopapa, S., et al. 2018, JQSRT, 217, 86
Waldmann, I. P., Tinetti, G., Drossart, P., et al. 2012, ApJ, 744, 35
Walsh, K. J., Morbidelli, A., Raymond, S. N., O'Brien, D. P., & Mandell, A. M. 2011, Natur, 475, 206
Wilkening, L. L., & Matthews, M. S. (ed.) 1982, Comets (Tucson, AZ: Univ. Arizona Press)